Symmetry energy effect on hot nuclear matter and proto-neutron stars*

Xuhao Wu (武旭浩)[1†] Peng-Cheng Chu (初鹏程)[2,3‡] Min Ju (琚敏)[4§] He Liu (刘鹤)[2,3¶]

[1]Key Laboratory for Microstructural Material Physics of Hebei Province, School of Science, Yanshan University, Qinhuangdao 066004, China
[2]Science School, Qingdao University of Technology, Qingdao 266000, China
[3]The Research Center of Theoretical Physics, Qingdao University of Technology, Qingdao 266033, China
[4]School of Science, China University of Petroleum (East China), Qingdao 266580, China

Abstract: We examine the effects of symmetry energy on proto-neutron stars (PNSs) using an equation of state (EOS) described by the relativistic mean-field (RMF) model. The thermal properties of dense matter and the bulk properties of PNSs are investigated under the assumptions of isothermy, isentropy, and fixed lepton fractions. The polytropic index is calculated at finite temperature, revealing a negative correlation with the maximum mass of a PNS that the EOS can support. The properties of PNSs during the heating and cooling stages along their evolutionary path are explored under different combinations of lepton fraction and entropy. We investigate the correlation between symmetry energy slope L and the properties of PNSs. As L increases, the radius of a PNS also increases; however, this effect diminishes with a growing lepton fraction in the isentropic case. These results indicate that nuclear symmetry energy and its density dependence play crucial roles in determining the properties of PNSs and their evolutionary stages.

Keywords: proto-neutron star, symmetry Energy, evolution stages

DOI: 10.1088/1674-1137/adaa58 **CSTR:** 32044.14.ChinesePhysicsC.49054102

I. INTRODUCTION

The equation of state (EOS), which relates pressure to energy density (or mass density), plays a key role in determining the global structure of cold neutron stars (NSs) that are older than a few minutes and have temperatures below 1 MeV [1, 2]. In contrast, when considering studies on thermal dynamics, such as core-collapse supernovae (CCSNe) [3−7], proto-neutron star (PNS) or proto-quark star evolution [8−13], and binary neutron star (BNS) mergers [14, 15], an EOS input with finite temperature (T) and a fixed lepton fraction (Y_L) that is not in weak equilibrium [2, 16] is required. At this point, pressure becomes a function of three thermodynamic parameters: density, temperature, and lepton fraction. In supernova simulations and PNSs, the typical temperature of nuclear matter can range from a fraction of 1 MeV to several tens of MeV. In CCSNe, electron-capture reactions cause significant neutronization, leading to a decrease in Y_L (which equals Y_p, the proton fraction). During the subsequent cooling of the PNS, β-equilibrium is approached as neutrinos become free. Prior to this, the presence of trapped neutrinos limits the minimum value of Y_L, which is usually less than that of symmetric nuclear matter, *i.e.*, $Y_L < 0.5$. To describe the PNS that forms following the CCSNe of massive stars, it is necessary to consider baryon number densities up to several times the nuclear saturation density, temperatures up to 100 MeV, and lepton fractions up to $Y_L \sim 0.4$.

It is well known that symmetry energy and its slope play a crucial role in the structure of cold NSs [2, 17−19]. During CCSNe and PNS evolution, the symmetry of nuclear matter changes differently compared to cold NS matter. The temperature and density dependence of the nuclear symmetry free energy, using microscopic two- and three-body nuclear potentials, was investigated in [20]. The sensitivity of symmetry energy at twice the saturation density as a control parameter of the properties of hot and dense matter was investigated in [21]. The influence of symmetry energy on hot nuclear matter for supernova simulations over time was examined in [22]. Symmetry energy becomes one of the most significant factors affecting the EOS of hot dense nuclear matter and the bulk properties of PNSs.

Received 22 December 2024; Accepted 15 January 2025; Published online 16 January 2025

* Supported by the National Natural Science Foundation of China (12305148, 11975132, 12205158), the Natural Science Foundation of Hebei Province, China(A2023203055), and the Natural Science Foundation of Shandong Province, China (ZR2023QA112, ZR2022JQ04, ZR2021QA037, ZR2019YQ01)

† E-mail: wuhaobird@gmail.com
‡ E-mail: kyois@126.com
§ E-mail: jumin@upc.edu.cn
¶ E-mail: liuhe@qut.edu.cn

In this paper, we analyze the symmetry energy effects on hot dense nuclear matter and the cooling stage of PNSs at finite temperature, entropy, and lepton fraction. We apply the TM1e model [23, 24] and the original TM1 model [3, 25, 26], both of which have identical properties for symmetric nuclear matter but exhibit different behaviors regarding symmetry energy. The TM1e model has a symmetry energy slope (L) of 40 MeV, significantly smaller than $L = 110.8$ MeV, found in the original TM1 model. By considering the dependence on temperature and symmetry energy, we examine the thermodynamic properties of PNS matter and its bulk characteristics. Our results show that the symmetry energy dependence can significantly influence the EOS of hot nuclear matter, polytropic index curve, and bulk properties and evolution stages of PNSs.

The paper is organized as follows. In Sec. II, we derive the theoretical formalism for PNS matter at finite temperature within the relativistic mean-field (RMF) model. In Sec. III, we present calculation results regarding the properties of PNS matter and PNSs themselves. Finally, in Sec. IV, we present a summary and conclusions.

II. HOT EQUATION OF STATE

To describe dense nuclear matter at finite temperatures, we employ the RMF theory, which agrees well with terrestrial experimental data and saturation properties. The Lagrangian reads [23, 24, 27, 28]

$$\begin{aligned}\mathcal{L}_{\rm RMF} = &\sum_{i=p,n}\bar{\psi}_{\rm i}\left\{{\rm i}\gamma_\mu\partial^\mu-(M+g_\sigma\sigma)\right.\\&\left.-\gamma_\mu\left[g_\omega\omega^\mu+\frac{g_\rho}{2}\tau_a\rho^{a\mu}\right]\right\}\psi_i\\&+\frac{1}{2}\partial_\mu\sigma\partial^\mu\sigma-\frac{1}{2}m_\sigma^2\sigma^2-\frac{1}{3}g_2\sigma^3-\frac{1}{4}g_3\sigma^4\\&-\frac{1}{4}W_{\mu\nu}W^{\mu\nu}+\frac{1}{2}m_\omega^2\omega_\mu\omega^\mu+\frac{1}{4}c_3\left(\omega_\mu\omega^\mu\right)^2\\&-\frac{1}{4}R^a_{\mu\nu}R^{a\mu\nu}+\frac{1}{2}m_\rho^2\rho^a_\mu\rho^{a\mu}\\&+\Lambda_{\rm v}\left(g_\omega^2\omega_\mu\omega^\mu\right)\left(g_\rho^2\rho^a_\mu\rho^{a\mu}\right)\\&+\sum_{l=e,\mu}\bar{\psi}_l\left({\rm i}\gamma_\mu\partial^\mu-m_l\right)\psi_l,\end{aligned}\tag{1}$$

where $W^{\mu\nu}$ and $R^{\alpha\mu\nu}$ are the antisymmetric field tensors associated with ω^μ and $\rho^{\alpha\mu}$, respectively.

The effective mass of nucleon is expressed as

$$M_N^* = M + g_\sigma\sigma.\tag{2}$$

The parameters of mass and coupling constants are listed in Table 1.

The baryon number density can be written as

$$n_i = \frac{1}{\pi^2}\int k^2\left(f_i^k - f_{\bar{i}}^k\right){\rm d}k,\tag{3}$$

with the Fermi-Dirac distribution functions expressed as

$$f_i^k = \frac{1}{1+\exp\left[\left(\sqrt{k^2+M_i^{*2}}-\nu_i\right)/T\right]},\tag{4}$$

$$f_{\bar{i}}^k = \frac{1}{1+\exp\left[\left(\sqrt{k^2+M_i^{*2}}+\nu_i\right)/T\right]},\tag{5}$$

where i and $\bar{i}$ denote the particle and antiparticle, respectively. Chemical potential μ_i reads

$$\mu_p = \nu_p + g_\omega\omega + \frac{1}{2}g_\rho\rho,\tag{6}$$

$$\mu_n = \nu_n + g_\omega\omega - \frac{1}{2}g_\rho\rho,\tag{7}$$

where ν_i is the effective chemical potential. For isothermal or isentropic nuclear matter, the conditions of chemical equilibrium and charge neutrality are satisfied; they can be expressed as

$$\mu_n = \mu_p + \mu_e,\ \mu_\mu = \mu_e,\tag{8}$$

$$n_p = n_e + n_\mu.\tag{9}$$

Concerning neutrino-trapped matter, the lepton fraction is set as $Y_L = \text{constant}$ together with the following chemical equilibrium,

$$\mu_n = \mu_p + \mu_e + \mu_{\bar{\nu}_e}.\tag{10}$$

In contrast, for neutrino-free matter, lepton fraction Y_L varies with the density under β-equilibrium.

For given number density n_b, temperature T (or en-

Table 1. Parameters for the TM1 and TM1e models [3, 23]. The masses are expressed in MeV.

Model	M	m_σ	m_ω	m_ρ	g_σ	g_ω	g_ρ	g_2 /fm^{-1}	g_3	c_3	Λ_v
TM1	938.000	511.198	783.000	770.000	10.0289	12.6139	9.2644	7.2325	0.6183	71.3075	0
TM1e	938.000	511.198	783.000	770.000	10.0289	12.6139	13.9714	7.2325	0.6183	71.3075	0.0429

tropy s), and fixed lepton fraction Y_L, the expressions for energy density, pressure, and entropy density can be obtained as follows:

$$\begin{aligned}\varepsilon =& \sum_{i=n,p}\frac{1}{\pi^2}\int\left(k^2+M_N^{*\,2}\right)^{1/2}k^2\left(f_i^k+f_{\bar{i}}^k\right)\mathrm{d}k\\&+\frac{1}{2}m_\sigma^2\sigma^2+\frac{1}{3}g_2\sigma^3+\frac{1}{4}g_3\sigma^4\\&+\frac{1}{2}m_\omega^2\omega^2+\frac{3}{4}c_3\omega^4\\&+\frac{1}{2}m_\rho^2\rho^2+3\Lambda_{\rm v}\left(g_\omega^2\omega^2\right)\left(g_\rho^2\rho^2\right)\\&+\sum_{l=e,\mu}\frac{1}{\pi^2}\int\left(k^2+m_l^2\right)^{1/2}k^2\left(f_l^k+f_{\bar{l}}^k\right)\mathrm{d}k,\end{aligned}\tag{11}$$

$$\begin{aligned}P =& \frac{1}{3}\sum_{i=n,p}\frac{1}{\pi^2}\int\frac{k^4}{\left(k^2+M_N^{*\,2}\right)^{1/2}}\left(f_i^k+f_{\bar{i}}^k\right)\mathrm{d}k\\&-\frac{1}{2}m_\sigma^2\sigma^2-\frac{1}{3}g_2\sigma^3-\frac{1}{4}g_3\sigma^4\\&+\frac{1}{2}m_\omega^2\omega^2+\frac{1}{4}c_3\omega^4\\&+\frac{1}{2}m_\rho^2\rho^2+\Lambda_{\rm v}\left(g_\omega^2\omega^2\right)\left(g_\rho^2\rho^2\right)\\&+\frac{1}{3}\sum_{l=e,\mu}\frac{1}{\pi^2}\int\frac{k^4}{\left(k^2+m_l^2\right)^{1/2}}\left(f_l^k+f_{\bar{l}}^k\right)\mathrm{d}k,\end{aligned}\tag{12}$$

and

$$\begin{aligned}s =& \sum_{i=n,p}\frac{1}{\pi^2}\int\mathrm{d}k\left[-f_i^k\ln f_i^k-\left(1-f_i^k\right)\ln\left(1-f_i^k\right)\right.\\&\left.-f_{\bar{i}}^k\ln f_{\bar{i}}^k-\left(1-f_{\bar{i}}^k\right)\ln\left(1-f_{\bar{i}}^k\right)\right]\\&+\sum_{l=e,\mu}\frac{1}{\pi^2}\int\mathrm{d}k\left[-f_l^k\ln f_l^k-\left(1-f_l^k\right)\ln\left(1-f_l^k\right)\right.\\&\left.-f_{\bar{l}}^k\ln f_{\bar{l}}^k-\left(1-f_{\bar{l}}^k\right)\ln\left(1-f_{\bar{l}}^k\right)\right].\end{aligned}\tag{13}$$

The free energy density reads

$$f=\varepsilon-Ts.\tag{14}$$

A newly born PNS contains trapped neutrinos. It has become a standard procedure to consider the lepton numbers as fixed. Along the evolutionary path from a PNS to a cold NS, the following snapshots are commonly used: (I) $S=1, Y_L=0.4$; (II) $S=2, Y_\nu=0$; (III) $S=0, Y_\nu=0$; these are similar values to those reported in [9, 29–31]. Here, $S=s/n_b$ represents the entropy per baryon, $Y_L=\frac{n_e+n_{\nu_e}+n_\mu+n_{\nu_\mu}}{n_b}$ is the number of leptons (including electrons, muons, and neutrinos) per baryon with trapped neutrinos, and Y_ν is the number of neutrinos per baryon, where $Y_\nu=0$ denotes the neutrino-free case.

III. Results

In this section, we present numerical results for PNS matter and bulk properties of PNSs under the assumptions of isothermy, isentropy, and fixed lepton fractions. Under isothermal conditions, the β-equilibrium and charge neutrality are satisfied without neutrinos. Under isentropic conditions, the neutrino-free ($Y_\nu=0$) or neutrino-trapping ($Y_L=$ constant*ant*) scenarios are considered.

A. Isothermal PNS matter

In Fig. 1, we represent pressure P as a function of baryon number density n_b at different temperatures using TM1e and TM1 parameter sets. Note that the thermal effect slightly increases pressure P by a few megaelectron volts across all densities. Therefore, the thermal effect decreases with density compared to the strong interaction among nucleons. The TM1e and TM1 results slightly differ as well, with the TM1 results being slightly stiffer at all temperatures T. We will show that these differences have a significant impact on the bulk properties of PNSs.

In Fig. 2, we represent isospin asymmetry $\delta=\frac{n_n-n_p}{n_n+n_p}$ (upper panel), symmetry energy $E_{\rm sym}$, and symmetry free energy $F_{\rm sym}$ (lower panel) as functions of baryon number density n_b at different temperatures in the range of $T=0\sim60$ MeV under isothermal conditions. $E_{\rm sym}$ and $F_{\rm sym}$ are calculated under the following approximation:

$$F_{\rm sym}=\frac{f}{n_b}(\delta=1)-\frac{f}{n_b}(\delta=0),\tag{15}$$

$$E_{\rm sym}=\frac{\varepsilon}{n_b}(\delta=1)-\frac{\varepsilon}{n_b}(\delta=0).\tag{16}$$

Except for the differences arising from symmetry energy slope L, the thermal effects for both TM1e and TM1 results are similar. Isospin asymmetry δ is notably sensitive to temperature T at low densities, while the thermal effects become weaken in the high-density region. At lower densities (approximately $n_b<0.15$ fm^{-3}), a significant decline in δ with increasing T indicates a transition to more symmetric matter. There is a tendency for δ to converge at high densities, where higher densities lead to isospin-symmetric stable PNS matter. In cold NS matter, the anti-β decay, *i.e.*, the neutralization procedure, can be explained in terms of reduction of the kinetic energy of electrons. Therefore, with increasing temperature, higher thermal energy density and higher electron kinetic energy are expected. This leads to an increase in electron number density, which in turn results in a higher proton number density to maintain charge equilibrium. Con-

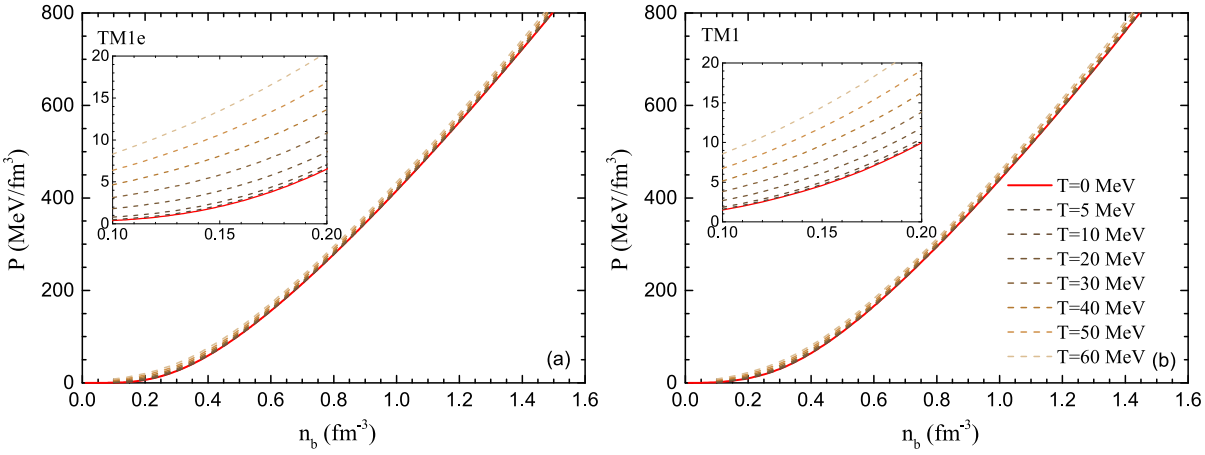

Fig. 1. (color online) Pressure P as a function of baryon number density n_b at different temperatures, $T = 0-60$ MeV, under β-equlibrium. The TM1e results are presented in the left panel whereas the TM1 results are represented in the right panel. Sub-figures show an enlargement of the low-density region results.

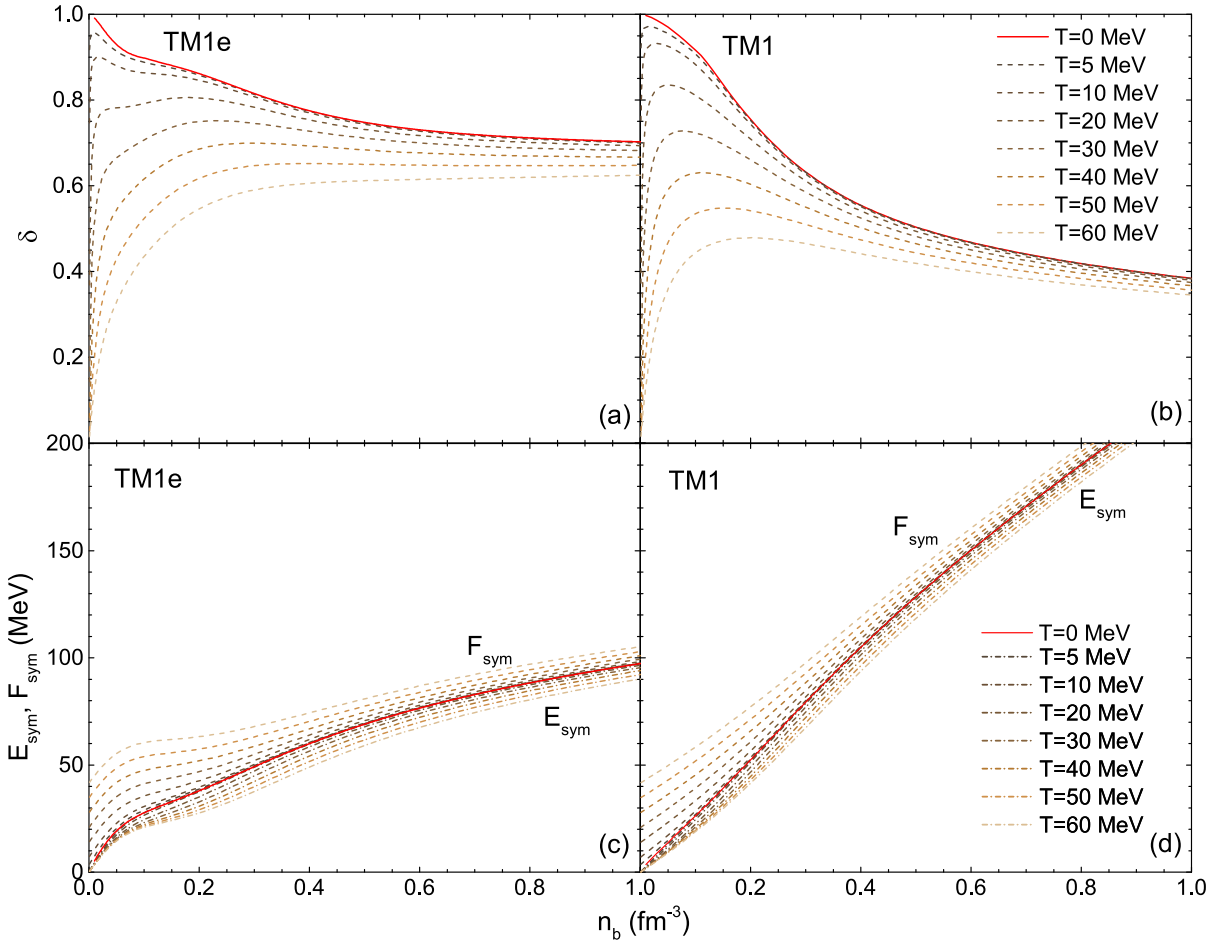

Fig. 2. (color online) Isospin asymmetry δ (upper panel), symmetry energy $E_{\rm sym}$ (dash-dot lines, lower panel), and symmetry free energy $F_{\rm sym}$ (dash lines, lower panel) as functions of baryon number density n_b under isothermal conditions ($T = 0-60$ MeV).

sequently, isospin asymmetry δ decreases with higher T. Compared to TM1 (which has a higher slope L) results, δ curves for TM1e (with lower slope L) level off more quickly. This difference is attributed to slope L of the symmetry energy. TM1e has a slightly smaller symmetry energy $E_{\rm sym}$ at the saturation density. This smaller L causes $E_{\rm sym}$ to increase smoothly compared to the TM1 results. In the low-density region, the thermal effect has a

greater impact on symmetry free energy $F_{\rm sym}$ than at high densities, while symmetry energy $E_{\rm sym}$ changes more gradually for different values of T. The finite temperature effect causes $E_{\rm sym}$ to decrease, while symmetry free energy $F_{\rm sym}$ increases (note that $E_{\rm sym} = F_{\rm sym}$ when $T = 0$). This indicates that the impact from nucleon isospin on the total energy density increases under finite temperature conditions.

In Fig. 3, we represent polytropic index γ as a function of baryon number density n_b at different temperatures; the expression employed for this representation is $\gamma = \partial(\ln P)/\partial(\ln\varepsilon)$. Note that with increasing temperature T, the curves of γ decrease, showing a similar trend to that of the isospin asymmetry δ. As T increases, the γ curves become smoother, especially in the low-density region. Despite the differences in symmetry energy slope between TM1e and TM1, both models exhibit a decrease in the polytropic index γ to approximately $\gamma \sim 1.1$ in the high-baryon-density region. This behavior arises because the isospin effect diminishes in the high-density regime as n_b increases. Additionally, γ decreases with temperature T at the same n_b, and the gap in γ curves caused by different values of T significantly decreases, approaching zero when $n_b > 0.6$ fm^{-3}. This change indicates a reduced thermal impact in the high-density region, which can be inferred from Fig. 1. The contribution of thermal effects to the total pressure diminishes as density increases, as does the fraction of energy density contributed by thermal effects. By contrast, in the low-density regions, the thermal contribution to pressure and energy density fraction is relatively significant. The similar shapes of the curves indicate that nucleon interactions play a decisive role in the EOS, especially at high densities. The thermal effect on the overall decline of γ suggests that the relationship between pressure and energy density becomes smoother. In Tables 2 and 3, we summarize the isothermal bulk properties of PNSs using the TM1e and TM1 models at different values of T. With the inclusion of thermal effects, both the maximum mass and radius increase with T, while the central density decreases. There exists minimum mass $M_{\rm min}$ for PNSs at high temperature T (at lower T, the minimum masses are positioned at very high radius values that are not included in Tables 2 and 3), as discussed in Refs. [32−34]. $M_{\rm min}$ is the minimum value below which a non-equilibrium state is reached. It may provide insights into the minimum mass of the resulting remnant NS after CCSNe. Our results show that minimum mass $M_{\rm min}$ increases rapidly with temperature T, such that for $T > 30$ MeV, $M_{\rm min}$ may exceed the maximum mass of PNSs. Beyond this temperature, the isothermal PNS is in a non-equilibrium configuration. Combining Fig. 3, Tables 2 and 3, it can be concluded that γ has a negative correlation with the maximum star mass at finite temperatures within the TM1e and TM1 models. The EOSs that can support larger maximum masses $M_{\rm max}$ are associated with lower γ curves. However, this relationship may not hold when considering different models, even though TM1e and TM1 differ only in their symmetry energy and slope.

B. Isentropic PNS bulk properties

In Fig. 4, we represent polytropic index γ as a function of baryon number density n_b at different values of the entropy per baryon S, considering both neutrino-free ($Y_{\nu_e} = 0$) and neutrino-trapping ($Y_L = 0.2, Y_L = 0.4$) conditions. As S increases, the curves of γ become less steep, particularly at lower densities, exhibiting a trend similar to that of the isothermal curves shown in Fig. 3. This behavior can also be attributed to the thermal effects under isentropic conditions, which lead to smoother changes in pressure relative to energy density.

A similar trend in the curves is observed at high densities. However, note that in the low-density region, $\gamma(Y_L = 0.2) > \gamma(Y_L = 0.4) > \gamma(Y_{\nu_e} = 0)$ for the same entropy

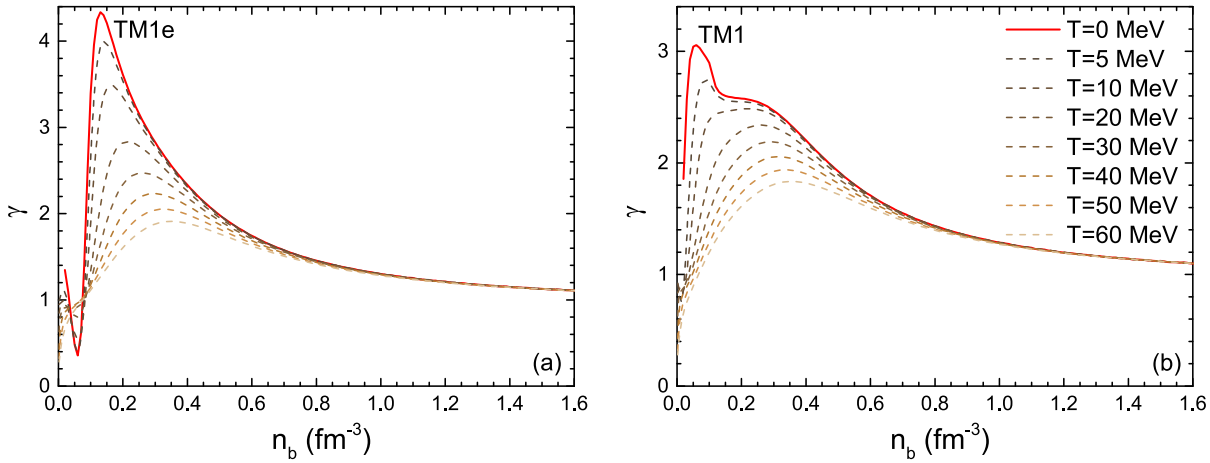

Fig. 3. (color online) Polytropic index γ as a function of baryon number density n_b at different temperatures, $T = 0 \sim 60$ MeV. The results are derived from the EOSs considered in Fig. 1.

Table 2. Summary of isothermal PNS bulk properties for the neutrino-free case and TM1e parameter set. $M_{\max}$ is the maximum mass; $R_{\max}$ and n_b^c are the corresponding radius and central density; $R_{1.4}$ is the radius of the canonical 1.4 $M_\odot$ PNS; $M_{\min}$ and $R_{\min}$ are the mass and radius of the minimum-mass PNS.

T/MeV	$M_{\max}$ /$M_\odot$	$R_{\max}$/km	n_b^c /fm^{-3}	$R_{1.4}$/km	$M_{\min}$ /$M_\odot$	$R_{\min}$/km
0	2.121	11.81	0.8959	13.02	–	–
5	2.125	12.19	0.8953	14.02	–	–
10	2.129	12.85	0.8949	16.18	–	–
20	2.147	15.28	0.8708	30.08	1.265	47.21
30	2.192	22.10	0.8234	–	2.041	43.21

Table 3. Same as Table 2 but for the TM1 parameter set.

T/MeV	$M_{\max}$ /$M_\odot$	$R_{\max}$/km	n_b^c /fm^{-3}	$R_{1.4}$/km	$M_{\min}$ /$M_\odot$	$R_{\min}$/km
0	2.178	12.37	0.8474	14.20	–	–
5	2.180	12.72	0.8473	15.34	–	–
10	2.185	13.43	0.8468	18.02	–	–
20	2.206	15.88	0.8449	–	1.406	46.51
30	2.259	23.91	0.7414	–	2.162	42.72

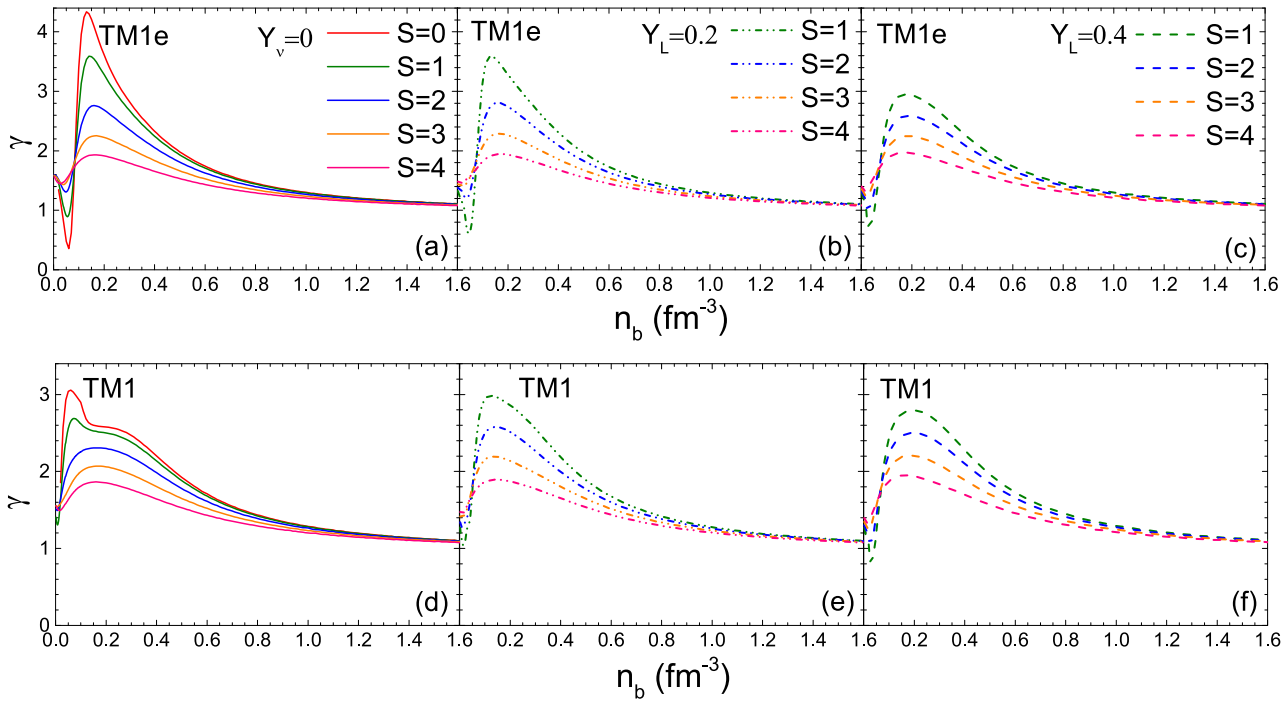

Fig. 4. (color online) Polytropic index γ as a function of baryon number density n_b at different values of entropy per baryon S, considering both neutrino-free ($Y_\nu = 0$, left panel) and neutrino-trapping scenarios ($Y_L = 0.2$ (middle pane), $Y_L = 0.4$ (right panel)).

per baryon S. The differences observed in the results for $Y_\nu = 0$, $Y_L = 0.2$, and $Y_L = 0.4$ are affected by the contributions to the pressure and energy density from neutrinos. The differences between the neutrino-trapping cases ($Y_L = 0.2$ and $Y_L = 0.4$) stem from the influence of the neutrinos on thermodynamic quantities and isospin. The latter is expected to be the primary factor, as $Y_L = 0.4$ corresponds to more symmetric PNS matter, resulting in slightly softer EOSs. In Tables 4 and 5, we summarize the isentropic PNS bulk properties using the TM1e and TM1 models under both neutrino-free ($Y_{\nu_e} = 0$) and neutrino-trapping ($Y_L = 0.2$ and $Y_L = 0.4$) conditions. As the entropy per baryon S increases, a heavier PNS is obtained with a smaller central density n_b^c but a higher central temperature T_c. A lower value of L (TM1e model) results in a higher central temperature T_c for the same S and

Table 4. Summary of isoentropic PNS bulk properties for neutrino-free ($Y_\nu = 0$) and neutrino-trapping ($Y_L = 0.2, 0.4$) conditions for the TM1e parameter set. T_c is the central temperature of the maximum-mass PNS.

Y_L	S/k_B	$M_{\max}/M_\odot$	$R_{\max}$/km	n_b^c/fm^{-3}	T_c/MeV	$R_{1.4}$/km
	0	2.121	11,81	0.896	0	13.02
ν	1	2.140	12.15	0.864	36.24	13.67
free	2	2.194	13.13	0.785	69.20	15.93
	3	2.296	15.08	0.660	93.94	21.89
	1	2.120	11.92	0.922	35.30	13.57
0.2	2	2.179	12.83	0.839	68.63	15.60
	3	2.281	14.64	0.703	91.72	20.84
	1	2.107	12.32	0.903	28.83	14.95
0.4	2	2.157	13.15	0.826	57.40	17.07
	3	2.230	14.73	0.705	82.70	21.97

Table 5. Same as Table 4 but for the TM1 parameter set.

Y_L	S/k_B	$M_{\max}/M_\odot$	$R_{\max}$/km	n_b^c/fm^{-3}	T_c/MeV	$R_{1.4}$/km
	0	2.178	12.37	0.847	0	14.20
	1	2.193	12.58	0.841	31.14	14.78
νfree	2	2.242	13.52	0.760	61.17	17.08
	3	2.339	15.40	0.642	86.89	23.05
	1	2.216	12.52	0.822	31.57	14.40
0.2	2	2.265	13.46	0.745	60.50	16.53
	3	2.357	15.18	0.651	84.10	21.85
	1	2.107	12.35	0.893	29.04	14.95
0.4	2	2.157	13.23	0.806	57.30	17.07
	3	2.253	14.84	0.698	82.24	22.43

Y_L. Also, in conjunction with Fig. 4, it can be concluded that γ exhibits a negative relationship with the increase in the maximum mass of a PNS under isentropic conditions. This relationship is specific to the same model (TM1e or TM1) and same isentropic conditions (either $Y_{\nu_e} = 0$ or same Y_L).

In Fig. 5, we represent temperature T as functions of n_b for $Y_\nu = 0$ and $Y_L = 0.4$ at $S = 1$ and $S = 2$. Note that the values of T significantly decrease with the density, especially near the PNS surface, where very low temperatures are evident. There are notable differences between the TM1e and TM1 results; specifically, TM1e exhibits a steeper increasing slope of T as a function of n_b. The effect of Y_L under the same entropy per baryon S is more pronounced for TM1e than for TM1, indicating a larger influence of the isentropic conditions due to the smaller symmetry energy slope L. However, with higher symmetry ($Y_L = 0.4$), the differences between TM1e and TM1 results become less significant. This can be easily explained: for symmetric nuclear matter ($Y_L = 0.5$), TM1e and TM1 yield the same EOS. Given that TM1 EOSs are slightly stiffer than those of TM1e (see Fig. 1), we can infer that, under isentropic conditions, stiffer EOSs are associated with lower temperatures for the same n_b.

In Fig. 6, we represent temperature T inside canonical 1.4 $M_\odot$ PNSs at the same stages as those considered in Fig. 5. Symbol r indicates the inner radius, distinguishing it from total radius R. The overall profile of T resembles the $T - n_b$ relations in Fig. 5 given that the canonical 1.4 $M_\odot$ PNSs have similar central densities ($n_c \sim 0.29 - 0.35$ fm^{-3}). For higher symmetry ($Y_L = 0.4$), TM1e and TM1 results have the same central density ($n_c = 0.298$ fm^{-3} for $S = 1$; $n_c = 0.35$ fm^{-3} for $S = 2$) and very similar T profile, as shown in Fig. 5. Concerning the neutrino-free scenario, TM1e leads to higher inner temperatures but an earlier temperature decrease when approaching the crust of the star. This is consistent with the fact that TM1 results in a thinner crust compared to TM1e [35] owing to differences in L.

In Fig. 7, we represent the mass-radius relations of PNSs at three isentropic stages along a PNS evolutionary

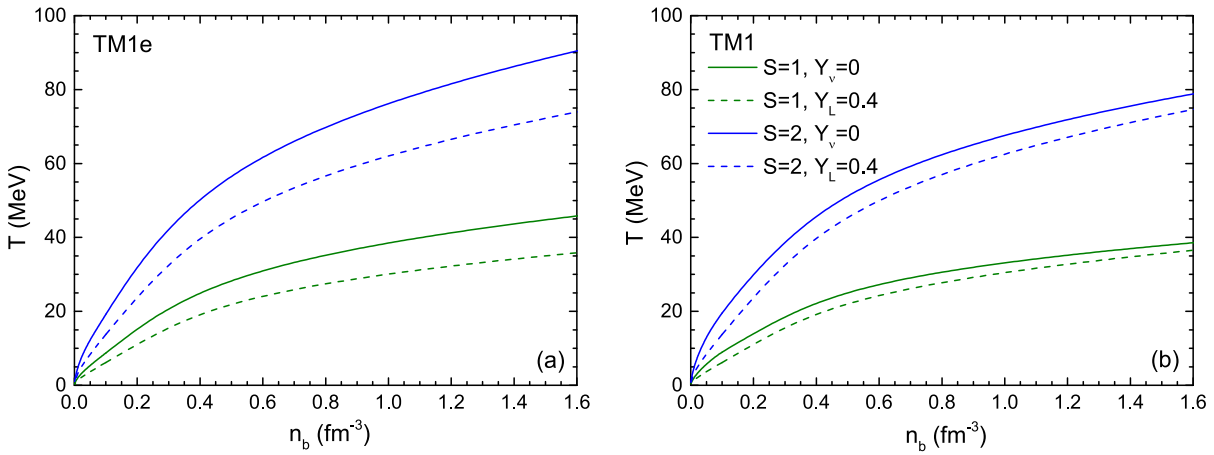

Fig. 5. (color online) Temperature T as a function of baryon number density n_b.

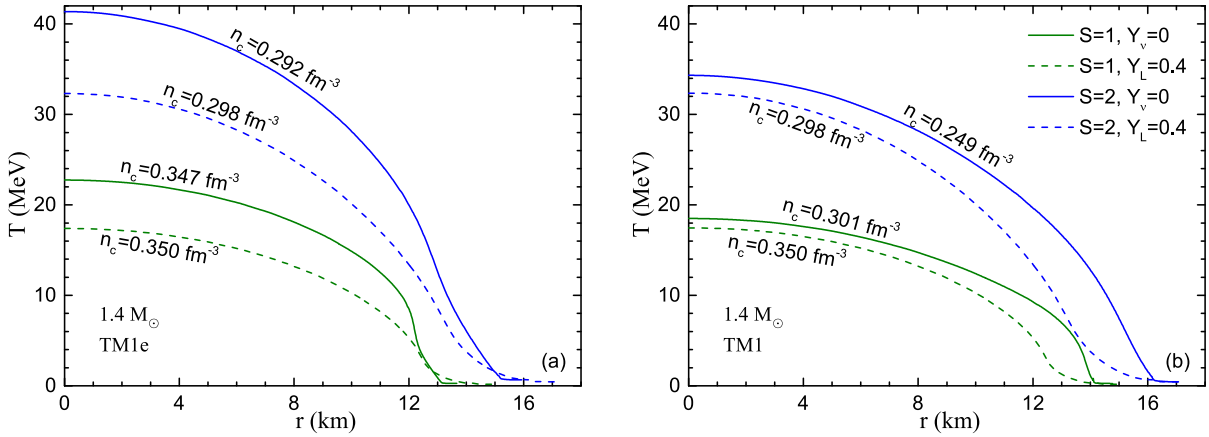

Fig. 6. (color online) Temperature T as a function of the inner radius (r) in the canonical 1.4 $M_\odot$ stars. Total radius of these stars $R_{1.4}$ are listed in Tables 4 and 5; n_c denotes the central density corresponding to the respective stars.

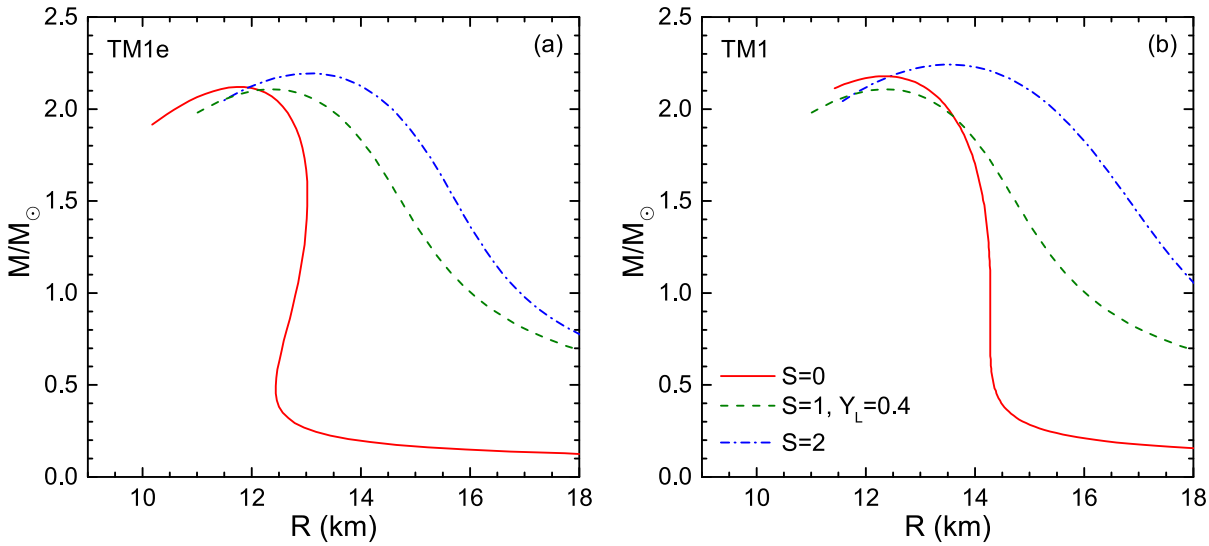

Fig. 7. (color online) Mass-radius relation at different isentropic stages along the PNS evolution line.

path, utilizing both the TM1e and TM1 models. Initially, during the heating stage, the PNS expands with increasing entropy per baryon S while experiencing a decrease in the lepton fraction Y_L, *i.e.*, it undergoes neutronization. As trapped neutrinos begin to escape, the star begins cooling. In the first stage of PNS evolution, with an entropy per baryon $S = 1$ and $Y_L = 0.4$, there is a significant presence of trapped neutrinos, resulting in a maximum mass of 2.107 $M_\odot$ applying the TM1e model, which is slightly smaller than the cold NS maximum mass of 2.121$M_\odot$. On the one hand, pure thermal effect leads to the stellar expansion, thereby allowing for a larger maximum mass and radius, shown by the $S = 2$ and $S = 0$ curves. Tables 4 and 5 show that in the neutrino-free case, the maximum mass increases with S. On the other hand, owing to the presence of trapped neutrinos, PNS matter exhibits greater symmetry compared to cold NS matter. More symmetric nuclear matter results in relatively lower nucleon interactions compared to asymmetric nuclear matter, consequently yielding a lower maximum mass. This relationship between the maximum masses in the neutrino-free and neutrino-trapping cases is further illustrated in Tables 4 and 5, where for the same S, higher lepton fraction $Y_L = 0.4$ (indicating more symmetric PNS matter) leads to a slightly diminished maximum mass compared to the cases $Y_L = 0.2$ or $Y_\nu = 0$. Comparing TM1 results with those of TM1e, the isentropic stage curves shift more significantly than those of the cold NS mass-radius relation. Aside from differences in symmetry energy (and its slope), TM1e predicts higher temperatures at the same density for equal S and Y_L, as shown in Fig. 5. Notably, temperature differences also stem from the variations in symmetry energy and its slope, as discussed in Fig. 5.

IV. SUMMARY

In this paper, we calculate the effect of symmetry en-

ergy on the EOS of hot nuclear matter and the bulk properties of PNSs. We employ the RMF framework and introduce two parameter sets, TM1e and TM1, which present the same saturation properties, differing only in symmetry energy and slope. To investigate the thermal effect, we consider the conditions of isothermy, isentropy, and neutrino trapping with fixed lepton fractions.

In the isothermal case, thermal effects directly contribute to the pressure but reduce both isospin asymmetry and symmetry energy. We found that the influence of thermal effects diminishes at high densities, where nuclear interactions become more significant. In the isentropic case, neutrinos contribute lesser to the thermodynamic quantities than electrons and muons. Additionally, a larger lepton fraction Y_L indicates a more symmetric nuclear matter environment, resulting in lower energy and pressure compared to neutrino-free nuclear matter. Under isentropic conditions, a rapid temperature decrease is observed near the crust of the PNS. A lower L (TM1e) leads to higher inner temperatures in the neutrino-free case.

We calculated the bulk properties of PNSs at finite temperature for different snapshot stages along the evolutionary path. Our findings indicate that the central density decreases with increasing temperature or entropy. Additionally, we observed that the polytropic index curve of the EOS exhibits a negative correlation with the maximum mass of the PNS within the same model, regardless of whether the case involves isothermy, isentropy, neutrino-free conditions, or neutrino trapping.

Overall, our results indicate that symmetry energy significantly influences the EOS, isospin asymmetry, polytropic index, and the properties of PNSs at finite temperatures and different evolutionary stages. Especially during the heating stage, the mass-radius relations differ considerably from those of cold NSs owing to the symmetry energy effect.

References

[1] Y. Suwa, Publ. Astron. Soc. Jpn. **66**, L1 (2014)
[2] M. Oertel, M. Hempel, and T. Klähn, and S. Typel, Rev. Mod. Phys. **89**, 015007 (2017)
[3] H. Shen, H. Toki, K. Oyamatsu *et al*., Prog. Theor. Phys. **100**, 1013 (1998)
[4] T. Yamasaki and S. Yamada, Astrophys. J. **887**, L21 (2006)
[5] C. Constantinou, B. Muccioli, M. Prakash *et al*., Phys. Rev. C **89**, 065802 (2014)
[6] Q. A. Mabanta and J. W. Murphy, Astrophys. J. **856**, 22 (2018)
[7] A. Burrows T. Wang, and D. Vartanyan, Astrophys. J. Lett. **964**, L16 (2024)
[8] M. Prakash, J. M. Lattimer, J. A. Pons *et al*., Lect. Notes Phys. **578**, 364 (2001)
[9] G.-Y. Shao, Phys. Lett. B **704**, 343 (2011)
[10] P.-C. Chu and L.-W. Chen, Phys. Rev. D **96**, 103001 (2017)
[11] A. R Raduta, M. Oertel, and A. Sedrakian, Mon. Not. R. Astron. Soc. **499**, 914 (2020)
[12] K. Sumiyoshi, S. Furusawa, H. Nagakura *et al*., Prog. Theor. Exp. Phys. **2023**, 013E02 (2022)
[13] P.-C. Chu, H. Liu, M. Ju *et al*., Phys. Rev. D **110**, 043032 (2024)
[14] M. Shibata and K. Taniguchi, Living Rev. Relativity **14**, 6 (2011)
[15] M. Ruiz, A. Tsokaros, and S. L. Shapiro, Phys. Rev. D **101**, 064042 (2020)
[16] S. Li, J. Pang, H. Shen *et al*., Astrophys. J. **980**, 54 (2025)
[17] C. Ducoin, J. Margueron, and C. Providência, Europhys. Lett. **91**, 32001 (2010)
[18] R. Cavagnoli, D. P. Menezes, C. Providência *et al*., Phys. Rev. C **86**, 065810 (2011)
[19] C. Providência and A. Rabhi, Phys. Rev. C **87**, 055801 (2011)
[20] C. Wellenhofer, J. W. Holt, and N. Kaiser, Phys. Rev. C **92**, 015801 (2015)
[21] K. Nakazato and H. Suzuki, Astrophys. J. **878**, 25 (2019)
[22] K. Sumiyoshi, K. Nakazato, H. Suzuki *et al*., Astrophys. J. **887**, 110 (2019)
[23] S. S. Bao, J. N. Hu, Z. W. Zhang *et al*., Phys. Rev. C **90**, 045802 (2014)
[24] H. Shen, F. Ji, J. N. Hu *et al*., Astrophys. J. **891**, 148 (2020)
[25] Y. Sugahara and H. Toki, Nucl. Phys. A **579**, 557 (2020)
[26] H. Shen, H. Toki, K. Oyamatsu *et al*., Astrophys. J. Suppl. Ser. **197**, 20 (2011)
[27] J. Meng, H. Toki, S. G. Zhou *et al*., Prog. Part. Nucl. Phys. **57**, 470 (2006)
[28] S. S. Bao and H. Shen, Phys. Rev. C **93**, 025807 (2016)
[29] A. W. Steiner, M. Prakash, and J.M. Lattimer, Phys. Lett. B **486**, 239 (2000)
[30] D. P. Menezes, A. Deppman, E. Megıas *et al*., Eur. Phys. J. A **51**, 155 (2000)
[31] P.-C. Chu, B. Wang, Y.-Y Jia *et al*., Phys. Rev. D **94**, 123014 (2016)
[32] P. Haensel, J. L. Zdunik, and F. Douchin, A&A **385**, 301 (2002)
[33] Y. Suwa, T. Yoshida, M. Shibata *et al*., Mon. Not. R. Astron. Soc. **481**, 3305 (2018)
[34] P. S. Koliogiannis and Ch. C. Moustakidis, Astrophys. J. **912**, 69 (2021)
[35] S. S. Bao and H. Shen, Phys. Rev. C **91**, 015807 (2015)